Pergamon

Atmospheric Environment Vol. 29, No. 16, pp. 2009–2018, 1995
Elsevier Science Ltd
Printed in Great Britain

1352–2310(94)00242–8

ROLE OF RADIATIVE TRANSFER IN MAINTENANCE AND DESTRUCTION OF STRATOCUMULUS CLOUDS

MARTIN J. LEACH and SETHU RAMAN

Department of Marine, Earth and Atmospheric Sciences, North Carolina State University, Raleigh, NC 27695-8208, U.S.A.

(*First received* 10 *March* 1993 *and in final form* 8 *May* 1994)

Abstract—A mesoscale numerical model is used to study the physical processes in the maintenance of a stratocumulus topped boundary layer. The model includes a surface energy budget, closure using a scheme based on the turbulence kinetic energy, a five category cloud physics scheme and radiative transfer. Model results demonstrate the role radiative flux divergence plays in the maintenance of a stratocumulus layer. Radiative heating and cooling of the cloud layer destabilizes the upper boundary layer and decouples that portion of the boundary layer from the surface layer. Eventually, sufficient solar radiation reaches the surface to overcome the decoupling and the cloud layer dissipates.

Key word index: Stratocumulus, radiative forcing, cloud physics, mesoscale circulation, boundary layer.

1. INTRODUCTION

Prediction of the future states of the climate is an important challenge imbedded in developing strategies for sustainable development. Expected warming due to anthropogenic activity may alter the frequency and amplitude of weather events and episodes including floods and droughts, extratropical storm tracks, tropical cyclones, El Nino, etc. The effects on agriculture, industrial activity and daily life may be dramatic. Great uncertainty remains in the physical processes currently included in the numerical models of the atmosphere used to forecast future climate. One of the greatest uncertainties is the interaction of clouds with radiative transfer. Low-level clouds increase the albedo of the atmosphere, leading to a cooling of the atmosphere. Higher clouds are more transmissive to short-wave radiation, but effectively trap longwave radiation, the so-called "greenhouse" or warming effect. At the same time, radiative flux divergence plays a role in the evolution of cloud systems, including cirrus shields from deep convective systems to the stratus and stratocumulus (Sc) clouds in the planetary boundary layer (PBL).

The United States Department of Energy has initiated the Atmospheric Radiation Measurement (ARM) program to address the uncertainties associated with the cloud/radiative transfer interaction. The first site in the U.S. southern great plains (SGP) was chosen because of the wide variety of cloud types that occur in that area, including Sc layers that develop in the wake of the massive convective systems that are frequent in that locale. An additional ARM site is expected to be along an eastern ocean boundary current, either off the west coast of Europe or the U.S. The primary reason for this future site is to study the marine Sc that form over the cold waters.

In the present study we use a two-dimensional numerical model to study the interaction of both shortwave and longwave radiative transfer with cloud water to determine its effect on the evolution of stratocumulus. The components of the model will be described in the next section. The simulations we performed are more germane to the Sc over the SGP as we also examine the interaction of the radiation with the land surface processes.

Lilly (1968) first suggested that stratocumulus clouds at the top of the boundary layer are maintained by negative buoyancy generated by radiative cooling at cloud top. The proper distribution of the longwave flux at the top of the Sc layers remains a problem in understanding the behavior and structure of Sc decks. Driedonks and Duynkerke (1989) recently reviewed the dynamics of stratocumulus layers and the progress and problems associated with modeling these climatologically important clouds. Strong temperature and liquid water gradients near the top of the cloud layer create difficulty calculating the radiative flux divergence. Observations suggest that the interface between cloud top and the air above is very sharp with thickness in the order of a metre, well below the resolution of existing numerical models. Longwave cooling also occurs in a small depth near cloud top where it is an important mechanism for the generation of turbulence in the ABL, at least in the Sc case. There is still some controversy about what happens in the entrainment zone. Entrainment often occurs over depths larger than the depth where the cooling occurs.

Deardorff (1976, 1981) suggests that part of the longwave cooling is located in the entrainment zone, thus cooling the entrainment zone directly without generating any new turbulence. However, Kahn and Businger (1979), argue that the cooling is associated only with the cloudy air and all of it generates cooling and contributes to the further generation of turbulence.

Albrecht (1981) used a simple model of trade wind boundary layer cumulus and concluded that radiative cooling of the boundary layer affects the amount of boundary layer cumulus, with lesser cloud amounts occurring with decreased radiative cooling. His study shows that trade-wind boundary layer cumulus is sensitive to both the sea surface temperature and radiative cooling in the boundary layer.

Heymsfield *et al.* (1991) used a stratocumulus model to study altocumulus. The principle driving mechanism for maintenance of the altocumulus layer was negative buoyancy driven by radiative cooling at cloud top, analogous to the mechanism driving stratocumulus suggested by Lilly. The calculations were compared to observations and the results indicate that radiation plays a critical role in dynamically unstable altocumulus clouds, with a lesser effect in stable clouds.

Duynkerke (1989) used a one-dimensional model to study the interaction between turbulence and radiation in the stratocumulus layer. An interesting finding is the decoupling of the subcloud layer and the cloud layer, showing how the radiation plays a pivotal role in this process. He compares model results to observations from two cases, November 16 and July 1 ("typical" cases from late fall and summer in midlatitudes). The turbulence in the boundary layer is driven by longwave radiative cooling at cloud top, except very near the surface, where wind shear is important. The IR cooling can be strong enough to promote mixing all of the way to the cloud top (the depth of the boundary layer). In the summer case, with a high sun angle, the shortwave radiative flux divergence (heating) approaches the same magnitude as the longwave radiative flux divergence (cooling) for the cloud layer as a whole. The shortwave radiative heating penetrates deeper in the cloud than longwave cooling, destabilizing the cloud. The net effect of the shortwave is to reduce the magnitude of the buoyancy flux in the cloud. At some point the buoyancy consumes, rather than produces TKE, suppressing turbulent mixing. The stable layer, because of the heating in the cloud, suppresses mixing from the surface and prevents moisture transport from the surface.

Duynkerke (1991) used a one-dimensional model to study the formation of radiation fogs. The model includes turbulence closure using K-theory, a vegetation and soil model, longwave radiation approximations, and a cloud droplet model including turbulent transport and gravitational settling of the fog droplets. He compared the model results to observations from a fall night in the Netherlands (16/17 October, 1988) and found that clear air radiative cooling is critical for fog formation. Radiative cooling was also found important in determining the overall structure of the boundary layer. The model simulation qualitatively agrees with observations but underestimates the heat fluxes.

2. DESCRIPTION OF THE MODEL

The model used in this study is a hydrostatic primitive equation model originally described by Huang and Raman (1992). The advection equations are solved using an upstream spline interpolation scheme in the horizontal with an upstream quadratic interpolation scheme in the vertical. The model includes TKE-ε closure after Mellor and Yamada (1982). Recent additions to the model include a surface energy balance incorporating soil moisture (Louis, 1979), a five category cloud physics scheme (Rutledge and Hobbs, 1983) and radiative transfer (Harshvardhan *et al.*, 1986) which includes both shortwave and longwave radiative transfer. The five categories in the cloud physics scheme are water vapor, cloud water, cloud ice, rain and snow. Mass continuity equations for the five categories are solved which include the effects of advection, conversion between the categories, and removal of water from the atmosphere due to falling rain and snow. The radiative transfer parameterization is broadband for both shortwave and longwave radiation. The scheme includes the effects of H_2O, CO_2, and O_3. Clouds are assumed radiatively black for longwave radiation in this study. Clouds are treated in the shortwave using a delta-Eddington approach. The extinction coefficient for cloud water is assumed to depend only on liquid water content. The optical depth of a cloud is the product of extinction and cloud depth. The extinction for cloud ice is assumed to be half of that for liquid water clouds.

3. DESCRIPTION OF THE EXPERIMENTS

Four case studies were conducted using the numerical model. The experiments were designed to study the interactive role of radiation with clouds in formation and maintenance of a stratocumulus layer. There were 241 horizontal grid points, with a grid increment of 5 km. The horizontal cross section is assumed to be eastwest with no change in the coriolis force. The vertical domain was 12 km, with 33 telescoping grid points. The finest vertical resolution of 50 m is near the surface with the coarsest resolution of 500 m for all layers above 3 km. The same initial temperature and moisture profile was used for all four cases. The surface temperature was 283 K, with a Brunt–Vaisala frequency of $0.0075\ s^{-1}$ used to define the temperature lapse rate. This corresponds to a potential temperature lapse rate of approximately $\pm 1.6\ K\ km^{-1}$. The moisture is initialized with a constant relative humidity of 85% below 10 km, 40% above 10 km. The wind is initialized with a surface wind of $-10\ m\ s^{-1}$ with a constant shear of $0.002\ s^{-1}$, leading to a zero wind level at 5 km for cases 1 and 2. The model imposes a no slip or $0.0\ m\ s^{-1}$ wind at the surface with Ekman balance, so in reality the maximum easterly wind is $-9.4\ m\ s^{-1}$ at about 0.75 km. The initial wind is zero in the

Table 1. The initial conditions for the four cases described in the text

	SFC TEMP (K)	RH (%)	WIND	RAD
Case 1	283	85	$-10\,m\,s^{-1}$, shear	Yes
Case 2	283	85	$-10\,m\,s^{-1}$	No
Case 3	283	85	0.0	Yes
Case 4	283	85	0.0	No

Note: the temperature is the initial surface temperature and decreases with height at approximately $1.6\,K\,km^{-1}$. RAD indicates atmospheric radiative transfer is included. The value of shear as defined in the text is $0.003\,s^{-1}$.

entire domain for cases 3 and 4. Atmospheric radiative transfer is included in cases 1 and 3. The Sun angle is for March 1 at latitude 34.1 in the Northern Hemisphere and all simulations are started at 0500 local time. The surface energy balance includes the radiation terms for cases 2 and 4, with longwave exchange with the first atmospheric level. The effect of clouds is included in cases 2 and 4 by increasing the albedo according to the amount of cloud water present, but there is no direct interaction of the clouds and radiation. The initial conditions for the four cases are summarized in Table 1.

A circulation is created in the model by imposing a heat source in the middle troposphere of $8\,K\,h^{-1}$ for 1 h. The heat source is bell shaped, both horizontally and vertically. The vertical half-width is 2.5 km centered at 5 km. The horizontal half-width is 20 km centered at grid point 121, or in the center of the domain. At the end of the hour, the heating is turned off. Clouds develop in response to the vertical velocity that results, and the cloud interaction with radiative transfer, shear and planetary boundary layer (PBL) can be studied. The u and w components of the wind at 1 h from case 1 are shown in Fig. 1. This emphasizes the atmospheric response to the imposed heat source. The u-component shows divergence aloft with convergence at low levels. The w component shows upward vertical motion in the region of the imposed heating, with compensating subsidence on either side. Recent theoretical results (Lin and Smith, 1986, Nicholls *et al.*, 1991) for the transient response to an imposed heat source indicate that gravity waves will propagate away from the center without large-scale forcing or sufficient instability to maintain the circulation. The situation is analogous to the decaying stage of large thunderstorms and mesoscale convective complexes. The v-component, which in the two-dimensional model arises solely from coriolis effects, is not shown, but is consistent with the other wind components in the two-dimensional model; there is cyclonic vorticity in the lower troposphere with anticyclonic vorticity in the region of upper-level divergence. The experiments described in this paper are designed to investigate the interaction of clouds, radiative effects and propagating gravity waves on the development of stratocumulus clouds.

4. RESULTS

4.1. *The effect of atmospheric radiative transfer*

The wind components for case 1 at 6 h are shown in Fig. 2. The existence of gravity waves is evident in both the u and w components. The propagating disturbances due to the initial heat source are the largest perturbations in the wind fields with the downshear gravity wave exiting the domain. The w component indicates the presence of several small amplitude, small wavelength gravity waves on the upshear side. The gravity waves are also evident in the u-component, where the up shear propagating wave is more vertically oriented than the downshear wave. The structure in the middle troposphere in the middle of the domain evident in both components especially on the upshear side is due to the interaction of the cloud ice field with the longwave radiation. It is an interaction of gravity waves, clouds and radiative flux divergence that leads to the development of a stratocumulus layer in this case. The interaction and effect of radiation is shown in Fig. 3. The figure includes cloud water and cloud ice ($g\,kg^{-1}$) and longwave and shortwave heating rates ($K\,d^{-1}$) 6 h into the simulation.

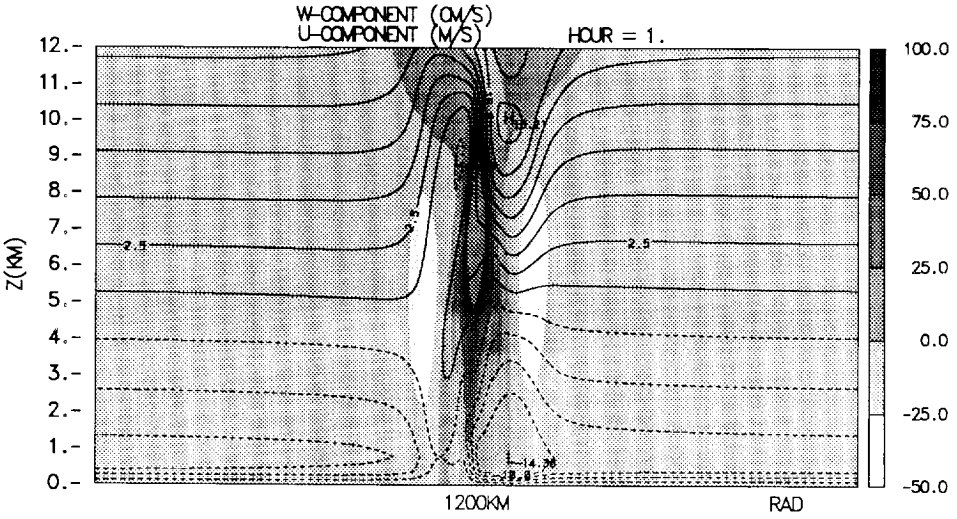

Fig. 1. The response of the wind field to the imposed heat source described in the text. The u component is represented by the contours with a contour interval of $2.5\,m\,s^{-1}$. The gray shades represent the w-component in $cm\,s^{-1}$. The label bar on the right shows the shading intervals.

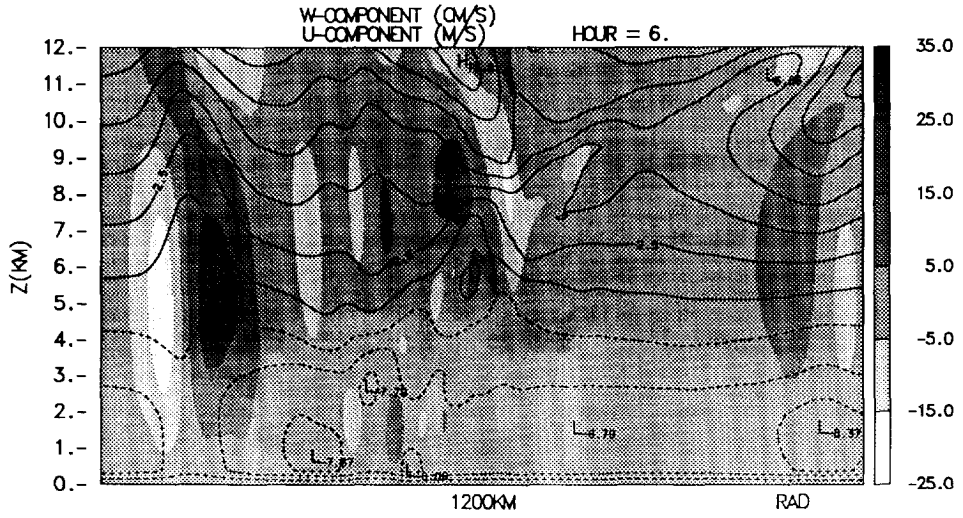

Fig. 2. The same as Fig. 1, but for 6 h into a simulation with radiative transfer included and the initial wind condition with shear. The contour interval for the u-component is the same as Fig. 1, but the shading interval for the w-component is reduced as shown in the label bar on the right.

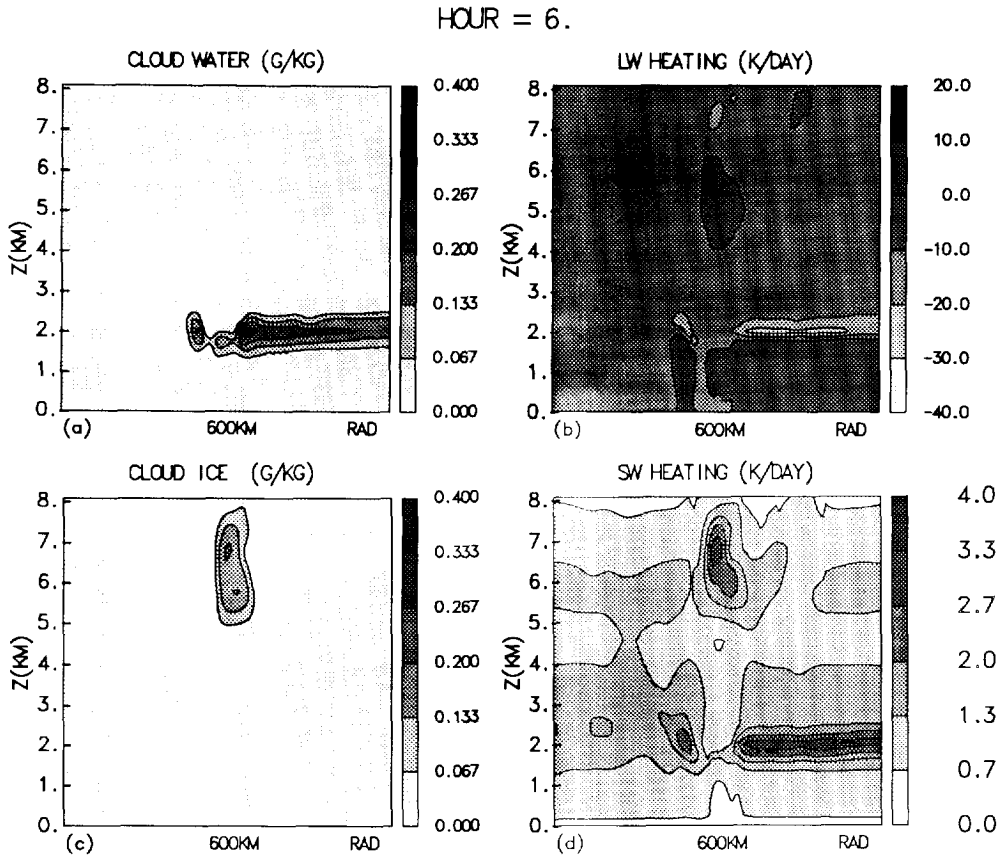

Fig. 3. Cloud water (a) and ice (c) mixing ratios and longwave (b) and shortwave (d) radiative heating rates for 6 h into the simulation. This corresponds to 1100 local time. The gray shade intervals for each plot are shown to the right of the plot. Cloud mixing ratios are ($g\,kg^{-1}$), radiative heating rates are $K\,d^{-1}$.

The gray-scale shading intervals are shown in the label bars on the right of each plot. These plots are from 1100 local time, or approximately the time of maximum shortwave heating. The stratus cloud layer is evident from the middle of the domain to the eastern or downshear boundary. There is also evidence of stratus clouds on the western side, but the stronger gravity wave driven downdrafts cause the clouds to be

discontinuous on this upshear side. The cloud ice that appears is at the top of the earlier updraft and does not advect as it appears at the level where the wind reverses direction. The longwave heating/cooling at the base/top of the stratus clouds and ice layer and the shortwave heating are shown in the figure. The radiation heating distribution is important for the maintenance of the stratocumulus layer. The clear areas are coincident with downdrafts and the areas where gravity waves remain active. The longwave heating at cloud base and cooling at cloud tops has several effects. First, it destabilizes the cloud layer, leading to longer lasting clouds with greater liquid water contents and effectively destroys the propagating gravity waves. Also, as pointed out by Duynkerke and Driedonks (1988) in their study of Sc in the North Atlantic it stabilizes the upper portion of the boundary layer, effectively decoupling the cloud layer from the surface forcing. The stabilization of the upper portion of the PBL is important for the Sc formation. By contrast, the cloud water and cloud ice from case 2 are shown in Fig. 4. The maximum concentration of cloud water is approximately seven times less than that shown in Fig. 3. Although there is less cloud water in the entire PBL, what is present is more evenly mixed through the depth of the PBL. In case 1, cloud water exists only near the top of a less deep PBL. The distribution of cloud ice is similar for the two cases, but without radiative transfer the maximum concentration is twice as large. Shortwave heating in the radiative transfer case enhances the melting process. The effect of no radiative transfer is evident. The upper portion of the PBL is not stabilized, allowing strong vertical mixing through the entire depth of the PBL. The lower cloud water amounts are due to an interactive process. Less clouds allow more solar radiation to reach the surface, heating the surface more, creating greater fluxes of sensible and latent heat, further destabilizing the PBL and creating greater mixing. Solar radiation reaching the surface eventually destroys the Sc layer. The cloud water amounts after 9 h from cases 1 and 2 are shown in Fig. 5. There is a striking similarity in cloud water distribution. Solar radiation penetrating the cloud layer in case 1 has sufficiently heated the surface to overcome the stability in the cloud layer, leading to the mixing process which dilutes the cloud water. The

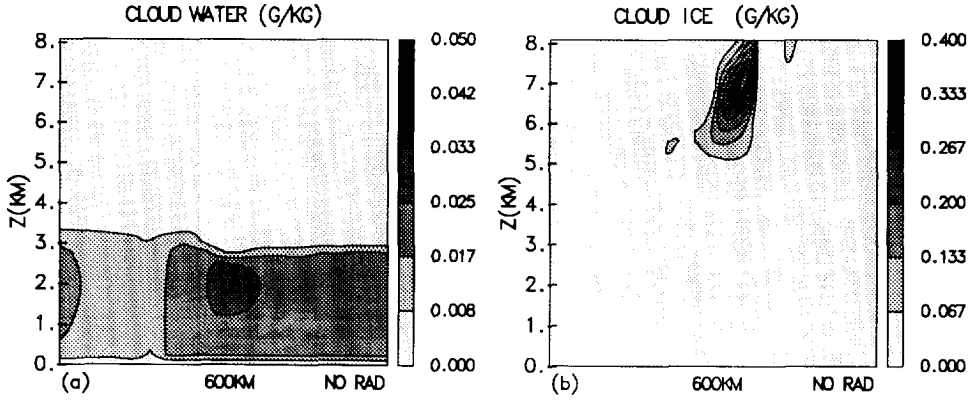

Fig. 4. Cloud water (a) and cloud ice (b) mixing ratios for 6 h into the simulation without radiative transfer. Note the reduction in the gray-scale shading interval for the cloud water mixing ratio.

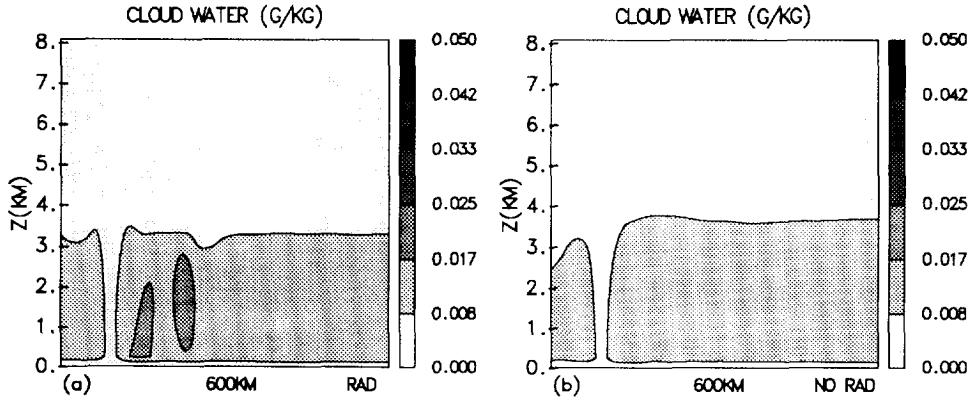

Fig. 5. Cloud water mixing ratio after 9 h simulation with radiative transfer (a) and without radiative transfer (b). The gray-shade intervals are on the right.

dilution comes from increasing the volume in which the cloud water is mixed and from heating the air, raising its saturation vapor pressure so that water condenses less easily.

Vertical profiles from the PBL at grid point 181 are shown in Fig. 6. Results from case 1 are shown in Fig. 6a with results from case 2 in Fig. 6b. Grid point 181 is the right boundary of the domain presented in the cross sections of the previous figures. Cloud water mixing ratio, longwave and shortwave heating rates and buoyancy production of TKE are shown. Each term is normalized by its maximum absolute value in the layer presented. The maximum values used for normalization of each quantity are in Table 2. The values in the table demonstrate greater buoyancy production in the PBL without radiative transfer, but with much smaller cloud water amounts. There is positive buoyancy production in the middle of the cloud layer when radiative transfer is included. Shortwave heating through the depth of the cloud layer, together with longwave cooling of the upper portion of the cloud destabilizes the top of the cloud layer, providing the local source of buoyancy. This effectively decouples the cloud layer from the well-mixed layer below. In case 2 (Fig. 6b), the buoyancy production is typical of a convectively growing boundary layer. Negative buoyancy at the top of the PBL delineates the entrainment zone, where air with greater θ_v is entrained into the PBL. The cloud layer is not decoupled from the well-mixed layer and the cloud water mixes through the entire depth of the PBL.

4.2. *The effect of no wind shear*

Results from case 3 shown in Fig. 7 demonstrate that shear also affects the evolution and distribution of the stratus clouds. There was no initial wind in this case. The stratus clouds now cover the entire domain with a maximum concentration approximately 12% greater than case 1 where shear was present. With shear, greater mechanical mixing contributes to the dilution of cloud water, leading to the smaller cloud amounts.

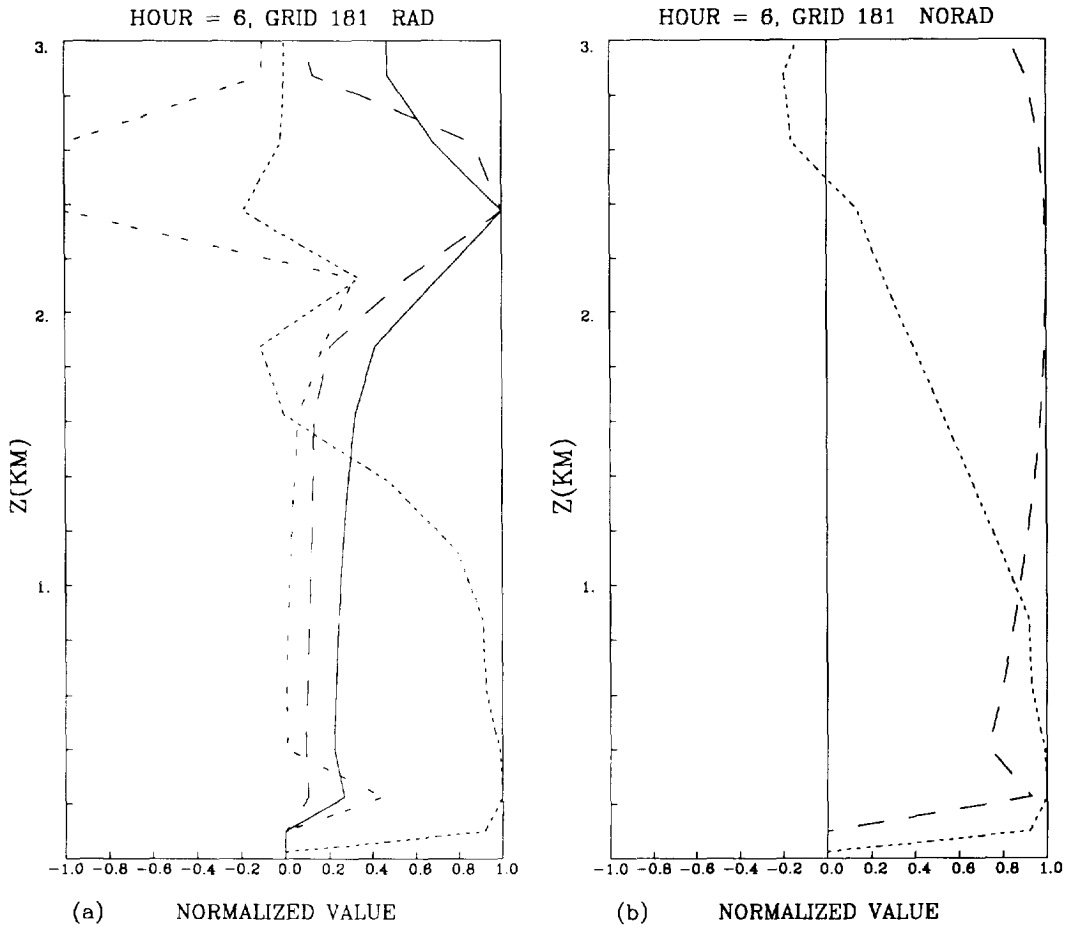

Fig. 6. Profiles of cloud water (long dashed), longwave heating (short dashed), shortwave heating (solid) and buoyancy production (dotted) at grid point 181, 6 h into the simulation. Grid point 181 is 1/4 into the domain from the right edge. The values are normalized by their maximum values. The panels are for the shear simulations with radiative transfer (a) and without radiative transfer (b).

Table 2. Normalization values used in Fig. 7 for the case with radiation and for the case without radiation

	RAD	NORAD
Buoyancy	6.5E-3 ($m^2 s^{-3}$)	9.3E-3
Cloud water	0.20 E-3 ($g kg^{-1}$)	0.23E-4
Shortwave heating	3.8 ($K d^{-1}$)	0.0
Longwave heating	19.3 ($K d^{-1}$)	0.0

4.3. *Interaction with surface processes*

The effect of the atmospheric radiative transfer on the surface energy budget is shown in Fig. 8. Without atmospheric radiative transfer, the albedo effect of clouds is included by calculating the total integrated liquid and ice water content of a column. A critical value of 1 $kg m^{-2}$ is assumed. Any column integrated water or ice content less than the critical value is assumed to have a cloud fraction equal to the ratio of the integrated value to the critical value. Values greater than the critical value become a cloud fraction of 1. The cloud effects on radiation are included following Kasten and Czeplak (1980):

$$R_S=(1-\alpha)R\downarrow(1+aF_c^b), \quad (1)$$

where $a=0.75$, $b=3.4$, F_c is the fractional cloudiness, α is surface albedo, $R\downarrow$ is the total downwelling shortwave radiation at the surface, and R_S is the absorbed shortwave radiation at the surface. Less shortwave radiation reaches the surface of the earth when atmospheric radiative transfer is explicitly included. The reduced shortwave at the surface is due to the inability of the Sc cloud layer to maintain itself through the longwave radiative flux divergence. The changes in the incident shortwave energy at the surface results in significant changes in all processes in the surface energy budget, including latent and sensible heat fluxes. This results in lesser generation of TKE, causing the PBL to grow at a smaller rate to lesser heights. A time sequence of the domain mean values of cloud water and cloud ice for cases 1 and 2 are shown in Fig. 9. The domain mean is calculated by multiplying each value in the domain by the density at the same point, multiplying by the depth that grid point represents, summing all values, then dividing by the total number of grid points. The units of the mean are $g m^{-2}$. Small values result from most of the domain being cloud free. From Figs 3 and 4, cloud water is confined to the PBL, cloud ice is present outside the PBL in the free atmosphere. The existence of cloud

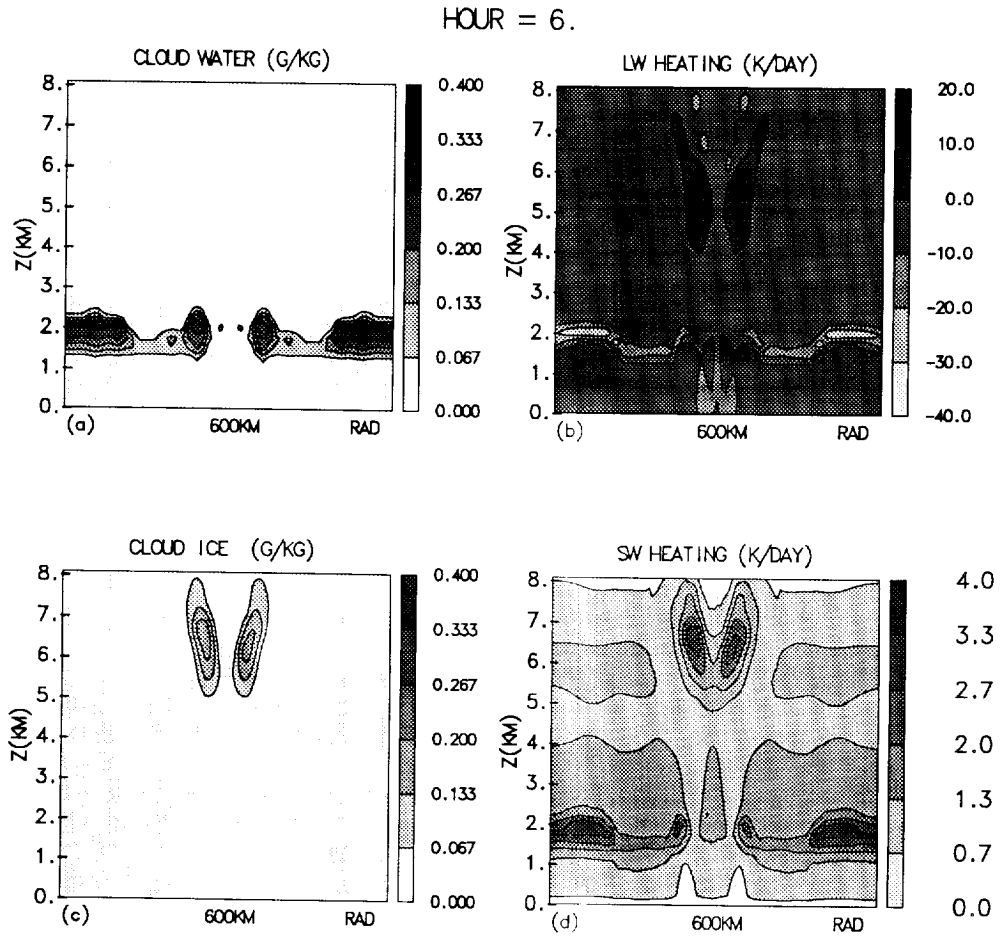

Fig. 7. The same as Fig. 3, but for the simulation when the initial wind is zero. Radiative transfer was included.

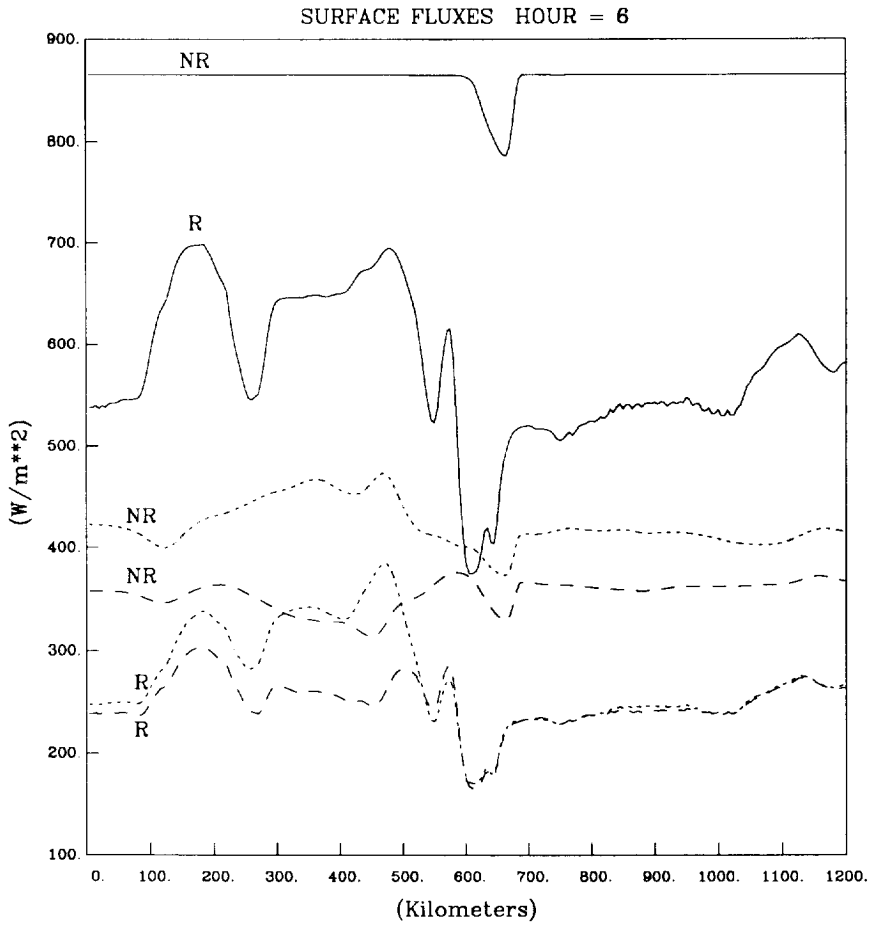

Fig. 8. The surface fluxes cases, 6 h into the simulations with shear included. The shortwave radiative fluxes are represented by the solid lines. The dotted lines are latent heat flux and the dashed lines are sensible heat flux. Curves representing values from the case including radiative are labeled *R*, those without radiative transfer are labeled NR.

water is evidence of PBL processes, specifically the decoupling of the surface layer from the upper portion of the PBL. More cloud water is present in case 1 at all times, demonstrating the effect of the radiative processes in maintaining the stratus clouds. For case 1, as solar heating continues after the times shown in the earlier figures, shortwave radiation reaching the surface creates enough heat flux to overcome the stabilization near the top of the PBL. A well-mixed layer similar to case 2 results with mixing of the cloud water through the entire depth of the PBL. Cloud ice is confined to the free atmosphere. Greater amounts for case 2 early in the simulation result from the lack of shortwave heating of the ice layer. The greater amounts for case 1 during the latter half of the simulation result from longwave radiative effects on the ice layer, similar to the stratocumulus forcing demonstrated in Fig. 3. Domain means, including surface fluxes, for all 4 cases are summarized in Table 3. The direct relationship of the surface heat fluxes to the downwelling shortwave radiation is apparent, as well as the indirect relationship of PBL cloud water to the amount of solar radiation reaching the surface. The maximum cloud amounts for cases 2 and 4 (no atmospheric radiative processes) occurs earlier and is related to the imposed heating. For the radiative cases (1 and 2), the maximum occurs later with the radiative decoupling of the surface layer maintaining the Sc layer.

5. SUMMARY AND CONCLUSIONS

An accurate representation of radiative transfer is imperative for climate modeling and therefore for developing strategies for future development. One of the great uncertainties in representing atmospheric radiative transfer in numerical models is related to the interaction of radiative flux divergence with clouds. It appears that radiative flux divergence contributes to the development, maintenance, and ultimately to the breakup of stratocumulus cloud layers.

Results demonstrate longwave radiative flux divergence at the cloud interface and shortwave heating in

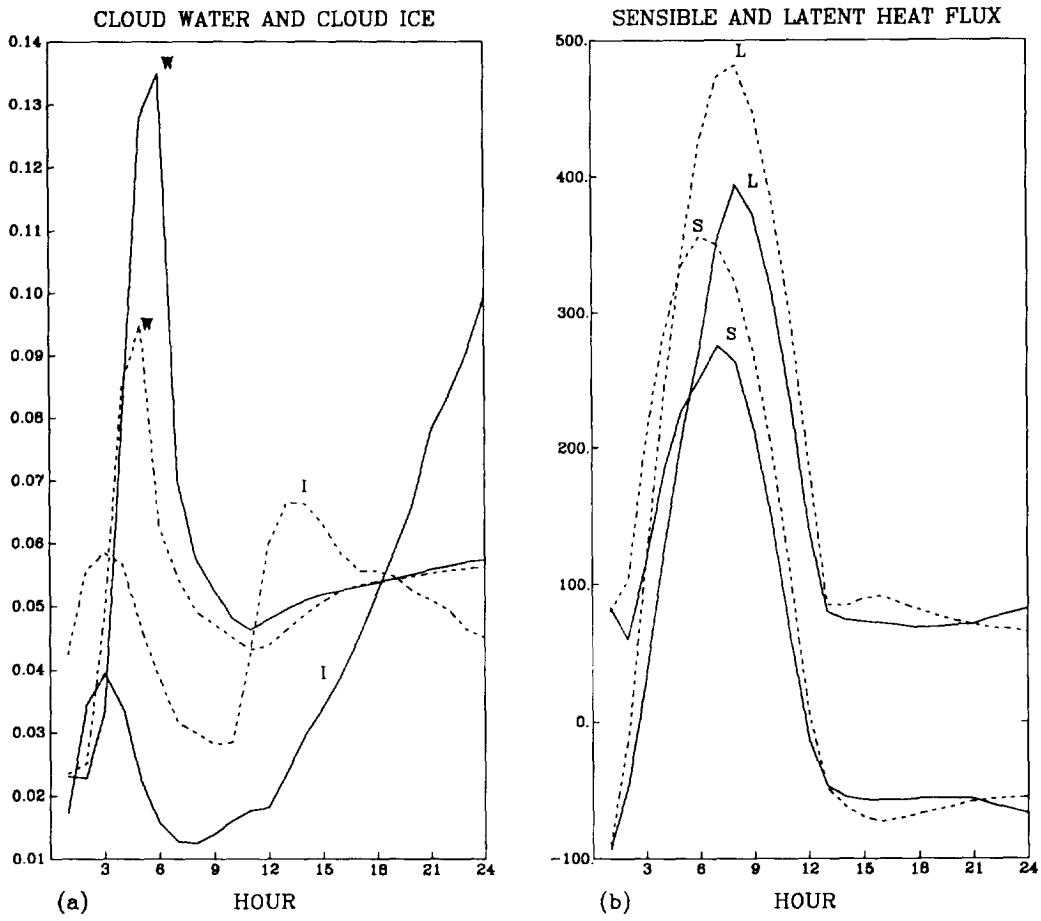

Fig. 9. Mean values for the entire domain for cloud water and cloud ice mixing ratios (a) and surface heat fluxes (b). The solid lines represent the case including radiative transfer, the dashed lines represent the case without radiative transfer. A *W* in (a) indicates cloud water and *I* indicates cloud ice. In (b), *L* indicates latent heat fluxes and *S* indicates sensible heat fluxes. The mixing ratio units are (kg m^{-2}) for the entire domain. The heat fluxes are in W m^{-2}.

Table 3. Domain means of cloud water, cloud ice and terms from the surface energy budget. For each cell, there are two entries: the maximum domain mean during 24 h of simulation, and the hour into the simulation when the maximum occurred (add 5 h for local solar time)

	q_c	q_i	SH	LH	SW	LWD	LWU
1	0.0041	0.0030	277	391	705	387	421
	6	24	7	8	8	10	8
2	0.0029	0.0018	358	480	900	394	436
	5	14	6	8	7	11	7
3	0.0050	0.0012	270	340	690	386	439
	6	3	8	8	8	11	8
4	0.0036	0.0012	370	430	900	392	456
	5	3	6	8	7	11	7

Note: The symbols q_c and q_i represent cloud water and cloud ice in g m^{-2}, SH, LH, SW, LWD, and LWU are sensible heat flux, latent heat flux, downwelling shortwave radiative flux, and downwelling and upwelling longwave radiative flux at the earth's surface. Units for all flux terms are W m^{-2}.

the cloud layer create a positive buoyancy flux in the top of the PBL. Negative buoyancy normally exists at the top of the PBL as air is entrained from the free atmosphere. The positive buoyancy flux effectively decouples the surface from the cloud layer until solar heating at the surface generates sufficient mixing to overcome the effect of the radiative flux divergence. There is an interaction of atmospheric radiative transfer with the terms in the surface energy budget. Clouds in the atmosphere reflect more shortwave energy,

allowing less to reach the earth's surface. This leads to less energy available to be partitioned into heat storage in the ground or into latent and sensible heat fluxes into the atmosphere. The planetary boundary layer is less energetic and mixing is less efficient. Once stratocumulus clouds exist at the top of the boundary layer, they help maintain their existence as they allow less solar energy to reach the surface. Shear also plays a role in the existence of Sc layers. Wind shear generates mechanical turbulence which produces mixing sufficient to destroy the buoyancy generation at the top of the boundary layer.

Both longwave and shortwave radiative flux divergence contribute to the development and maintenance of stratocumulus clouds. Shortwave radiation at the surface creates buoyant mixing which ultimately leads to the destruction of these clouds over land. Wind shear also contributes to the destruction of these boundary layer clouds as mechanical production of turbulence enhances the mixing process that leads to their breakup. Further studies will examine the marine boundary layer and sensitivity to optical depth.

Acknowledgements— We would like to thank Professor Harshvardhan of Purdue University for providing the radiative transfer code. This work was supported by the U.S. Department of Energy, Atmospheric Radiation Measurement Program (ARM) under contract 091575-A-Q1 with Pacific northwest Laboratories. The computer time for the simulations was provided by the North Carolina Supercomputing Center and the National Energy Research Supercomputer Center.

REFERENCES

Albrecht B. A. (1981) Parameterization of trade-cumulus amounts. *J. atmos. Sci.* **38,** 97–105.

Albrecht B. A. (1989) Aerosols, cloud microphysics, and fractional cloudiness. *Science* **245,** 1227–1230.

Chen S. and Cotton W. R. (1988) The sensitivity of stimulated extratropical mesoscale convective system to longwave radiation and ice-phase microphysics. *J. atmos. Sci.* **45,** 3897–3910.

Churchill D. D. and Houze R. A. Jr (1991) Effects of radiation and turbulence on the diabatic heating and water budget of the stratiform region of a tropical cloud cluster. *J. atmos sci.* **48,** 903–922.

Deardorff J. W. (1976) On the entrainment rate of a stratocumulus-capped mixed layer. *Boundary-Layer Met.* **25,** 289–321.

Deardorff J. W. (1981) On the distribution of mean radiative cooling at the top of a stratocumulus-capped mixed layer. *Q. J. R. met. Soc.* **107,** 191–202.

Driedonks A. G. M. and Duynkerke P. G. (1989) Current problems in the stratocumulus-tropped atmospheric boundary layer. *Boundary-Layer Met.* **46,** 275–303.

Dudhia J. (1989) Numerical study of convection observed during the winter monsoon experiment using a mesoscale two-dimensional model. *J. atmos. Sci.* **46,** 3077–3106.

Duynkerke P. G. and Driedonks A. G. M. (1988) Turbulent structure of a shear-driven stratus-topped atmospheric boundary layer: a comparison of model results with observations. *J. atmos. Sci.* **45,** 2343–2351.

Duynkerke P. G. (1989): The diurnal variation of a marine stratocumulus layer: a model sensitivity study. *Mon. Wea. Rev.* **117,** 1710–1725.

Duynkerke P. G. (1991) Radiation fog: a comparison of model stimulation with detailed observations. *Mon. Wea. Rev.* **119,** 324–341.

Harshvardhan., Davies R., Randall D. A. and Corsetti T. G. (1987) A fast radiation parameterization for atmospheric circulation models, *J. geophys. Res.* **92,** 1009–1016.

Heymsfield A. J., Milosevich L. M., Slingo A., Sassen K. and Starr D. O. C. (1991) An observational and theoretical study of highly supercooled altocumulus. *J. atmos. Sci.* **48,** 923–945.

Huang C.-Y. and Raman S. (1992) A three-dimensional numerical investigation of a Carolina coastal front and the Gulf stream rainband. *J. atmos. Sci.* **49,** 560–584.

Kahn P. H. and Businger J. A. (1979) The effect of radiative flux divergence on entrainment of a saturated convective boundary layer. *Q. J. R. met. Soc.* **105,** 303–385.

Kasten F. and Czeplak G. (1980) Solar and terrestrial radiation dependent on the amount and type of cloud. *Sol. Energy* **24,** 177–189.

Lilly D. K. (1968) Models of cloud-topped mixed layers under a strong inversion. *Q. J. R. met. Soc.* **94,** 292–309.

Lin Y.-L. and Smith R. B. (1986) Transient dynamics of airflow near a local heat source. *J. atmos. Sci.* **43,** 40–49.

Louis J. F. (1979) A parametric model of vertical eddy fluxes in the atmosphere. *Boundary Layer Met.* **17,** 187–202.

Mellor G. L. and Yamada T. (1982) Development of a turbulence closure model for geophysical fluidproblems. *Rev. geophys. Space Phys.* **20,** 851–875.

Nicholls M. E., Pielke R. A. and Cotton W. R. (1991) Thermally forced gravity waves in an atmosphere at rest. *J. atmos. Sci.* **48,** 1869–1884.

Rutledge S. A. and Hobbs P. V. (1983) The mesoscale and microscale structure and organization of clouds and precipitation in midlatitude cyclones. VIII: a model for the "seeder–feeder" process in warm-frontal rainbands *J. atmos. Sci.* **40,** 1185–1206.